SPR-enhanced fluorescence and protein-improved blood compatibility of quadruple core/shell nanostructure of $Ag@SiO_2@Eu^{3+}(tta)_3Phen@Protein$

Peipei Yan[1], Jianguo Tang[1] ✉, Yu Zhang[1], Wenfei Shen[1], Yao Wang[1], Lin Hou[2], Runhua Tian[2,3], Yanxin Wang[1], Haidong Li[1], Linjun Huang[1], Laurence A. Belfiore[1,4]

[1]*Institute of Hybrid Materials, National Center of International Joint Research for Hybrid Materials Technology, National Base of International Scientific & Technological Cooperation on Hybrid Materials, Qingdao University, 308 Ningxia Road, Qingdao 266071, People's Republic of China*
[2]*Biochemistry and Molecular Biology Department, School of Medicine, Qingdao University, 308 Ningxia Road, Qingdao 266071, People's Republic of China*
[3]*Department of Clinical Laboratory, The Affiliated Hospital of Qingdao University, 16 Jiangsu Road, Qingdao 266000, People's Republic of China*
[4]*Department of Chemical and Biological Engineering, Colorado State University, Fort Collins, CO 80523, USA*
✉ *E-mail: tang@qdu.edu.cn*

Published in Micro & Nano Letters; Received on 16th March 2018; Revised on 3rd May 2018; Accepted on 21st June 2018

This study presents a quadruple core/shell nanostructure of $Ag@SiO_2@Eu^{3+}(tta)_3Phen@Protein$ with both excellent fluorescent property and blood compatibility. Surface-plasma resonance (SPR) was utilised to enhance the fluorescence of europium (Eu^{3+}) complexes. In this situation, the fluorescence of $Eu^{3+}(tta)_3Phen$ in the triple $Ag@SiO_2@Eu^{3+}(tta)_3Phen$ nanostructure is greatly enhanced. To increase the biocompatibility in blood, lysozyme was used to modify the surface of the above triple nanostructure to get the quadruple nanostructure of $Ag@SiO_2@Eu^{3+}(tta)_3Phen@lysozyme$. Then, through the clinical anti-coagulation tests in human blood, the blood compatibility of $Ag@SiO_2@Eu^{3+}(tta)_3Phen@lysozyme$ is largely improved comparing with the triple nanostructure of $Ag@SiO_2@Eu^{3+}(tta)_3Phen$, and the values of PT-S, APTT-S, TT-S, and AT-III of quadruple nanostructure blood sample with the modification of protein have the high correlation coefficients, 0.993–0.994, which means that the quadruple nanostructure of $Ag@SiO_2@Eu^{3+}(tta)_3Phen@lysozyme$ is close to the anti-coagulation property of physiological saline state (0.9% NaCl aqueous solution). Thus, this work provides two key properties of the quadruple nanostructure of $Ag@SiO_2@Eu^{3+}(tta)_3Phen@lysozyme$: the excellent fluorescence and the outstanding blood compatibility. This nanomaterial can be applied to bio-imaging and bio-sensing in blood.

1. Introduction: Europium(III) (Eu^{3+}) included materials have sharp emission and long lifetime because of its forbidden f–f transitions [1, 2]. However, the weak interaction with its environment is a disadvantage. Therefore, 'photon antenna' is required to capture incoming photons to broaden its light absorption range and enhance its luminescent intensity [3, 4]. The compound to enhance the photo-acceptor is named 'antenna' [5]. A series of ligands with rare earth ions can be applied in the field of clinical medicine antibacterial and biological fluorescence labelling [6–8] As effective one, the β-diketonates have been intensively studied to apply for Eu^{3+} luminescent materials because of their coordination characteristic of the di-dentate structure of carboxyl group [9, 10]. 2-Thenoyltri-fluoroacetone (TTA) belongs to β-diketonate compounds, which can coordinate with Eu^{3+} and obtain red electroluminescent (emission peak about 610 nm) because their excited triplet energy level can match the f-electron energy level of Eu^{3+} at excited state well [11, 12]. The use of 1,10-phenanthroline monohydrate (Phen) can stabilise the complex structure and reduce the non-radiative de-excitation [13, 14]. Therefore, $Eu^{3+}(tta)_3Phen$ complex is an effective red light luminescent material. However, the incident light of light source may bleach the fluorescent emission in the application, and thus the further fluorescent enhancement is needed normally. Substantial research efforts have shown that the metallic nanoparticles can enhance the fluorescence intensities of Eu^{3+} [15], through which the radiative decay rates can be extended and fluorescence quantum yields of lanthanide complexes can be greatly enhanced by the surface plasmon resonance(SPR) effect of metallic nanoparticles. Unfortunately, researchers reported that naked metallic nanoparticles have a negative influence to it [16, 17]. In some studies, it revealed that encapsulating the metallic nanoparticles with a dielectric material (SiO_2) is a useful way to prohibit this electron transfer [14]. The thickness of 10–25 nm can achieve the most suitable fluorescence enhancement effect [18, 19]. Based on the core/shell structure of $Ag@SiO_2$, $Eu^{3+}(tta)_3Phen$ complex can further modify at the SiO_2 surface as the second shell, in which the fluorescence of $Eu^{3+}(tta)_3Phen$ complex can be enhanced by the SPR effect of nanosilver [20, 21].

The enhanced fluorescence of $Ag@SiO_2@Eu^{3+}(tta)_3Phen$ nanoparticles have a widely potential bio-imaging application [22, 23]. However, a series of difficulties need to be overcome. First, the surface property of $Ag@SiO_2@$ $Eu^{3+}(tta)_3Phen$ determines their dispersion in blood or in tissues. Second, the negative effects of blood and tissues should be avoided [24, 25]. Therefore, the surface modifications are the way of what researches do currently. Compared with Deng's team [26], our study focuses on using cheaper ligand materials to obtain the nanoparticles with a fluorescence enhancement effect and excellent anti-hemagglutination.

What we think to make biocompatible $Ag@SiO_2@$-$Eu^{3+}(tta)_3Phen$ nanoparticles is to use protein as a modification agent. Lysozyme is a popular protein, which can behave antibacterial, anti-inflammatory and antiviral effects [27, 28]. On the other hand, the grafting of lysozyme onto the surface of $Ag@SiO_2@Eu^{3+}(tta)_3Phen$ nanoparticles is possible because the functional groups in lysozyme structure can form coordination interaction with Eu^{3+} ions at the surface of above triple core/shell nanoparticles, $Ag@SiO_2@Eu^{3+}(tta)_3Phen$ [29]. First, in the structure of the $Eu^{3+}(tta)_3Phen$, the TTA and Phen can form the first shell to cover the surface of the Eu^{3+}, which make the conjugated group of the TTA and Phen have the org–org interaction with the amide bond of lysozyme [30, 31]. At the same time, the polar nitrogen and fluorine atom of the ligands can also produce the polar–polar interaction with the lysozyme [32, 33].

In this work, we present a quadruple core/shell nanostructure of $Ag@SiO_2@Eu^{3+}(tta)_3Phen@Protein$ with both good fluorescent property and blood compatibility. Through the measurements of anti-coagulation for clinical human blood, this quadruple nanostructure shows very close correlation coefficients with the referring agent of the physiological saline state (0.9% NaCl aqueous solution), which means the good blood compatibility.

2. Materials and methods

2.1. Materials: Eu_2O_3 (99.99%), ammonia ($NH_3{\cdot}H_2O$, 25–28%), $AgNO_3$, polyvinylpyrrolidone (PVP), glucose, sodium citrate, tetraethoxysilane (TEOS), ethanol, 2-thenoyltrifluoroacetone (TTA), 1,10-phenanthroline monohydrate (Phen), methanol, dimethyl sulfoxide (DMSO), phosphate buffered saline buffer (PBS, PH = 7.2), were purchased from Sinopharm Chemical Reagent Co. Ltd., China. Lyophilised hen egg white lysozyme (HEWL, HR7-110,) was purchased from Hampton Research, USA.

2.2. Methods

2.2.1. Preparation of $Ag@SiO_2$ nanoparticles: The experimental process is shown in Fig. 1*a*. 0.159 g PVP, 0.051 g sodium citrate and 0.083 g glucose were added to 30 ml water. After heated to 103°C, 5 ml $AgNO_3$ aqueous solution (3×10^{-4} mol/l) was added to the solution stirring for 2 h. Silver nanoparticles were obtained after cooling.

The $Ag@SiO_2$ core/shell nanoparticles can be obtained by the modified Stöber method [33]. 7.2 ml of silver colloid containing 80 ml ethanol, 2.7 ml ammonia and 9.2 ml water was heated to 40°C. 1 ml 10 mmol/l TEOS ethanol solution was added within 2 h under vigorous stirring. The $Ag@SiO_2$ nanoparticles were collected by centrifugation.

2.2.2. Preparation of triple nanostructure of $Ag@SiO_2@Eu^{3+}(tta)_3Phen$: Europium chloride ($EuCl_3{\cdot}6H_2O$) was prepared by the previous article [34]. The $EuCl_3{\cdot}6H_2O$ was dissolved to get the 2×10^{-3} mol/l solution in the methanol. The methanol solutions of TTA (6×10^{-5} mol) and Phen (2×10^{-5} mol) were obtained. Then, we took TTA and Phen solutions and dropwise into 9 ml methanol. After adjusting pH to 7.5, 200 µl $EuCl_3{\cdot}6H_2O$ solution (2×10^{-3} mol/l) was added to the solution. After stirred for 1 h at 40°C, $Eu(tta)_3Phen$ complex solution was obtained. The structure of the $Eu(tta)_3Phen$ is shown in Fig. 1*b*. Then 1 ml $Ag@SiO_2$ core/shell nanoparticle solution (1.6×10^{-5} mol) was added. After the process, the solution was heated at 40°C for 3 h under stirring.

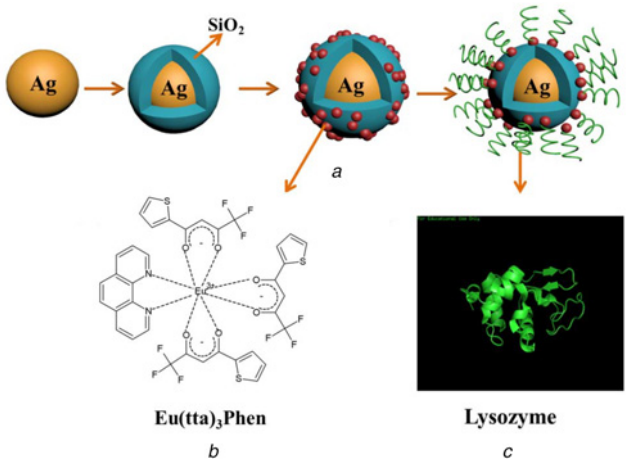

Fig. 1 *Synthesis scheme of quadruple core/shell nanostructure of $Ag@SiO_2@Eu^{3+}(tta)_3Phen@lysozyme$ complexes*
a Synthetic procedure of the $Ag@SiO_2@Eu^{3+}(tta)_3Phen@lysozyme$
b Structure of the $Eu^{3+}(tta)_3Phen$ complexes
c Structure diagram of lysozyme

2.2.3. Preparation of quadruple core/shell nanostructures of $Ag@SiO_2@Eu^{3+}(tta)_3Phen@lysozyme$: The structure of the lysozyme is shown in Fig. 1*c*. The prepared $Ag@SiO_2@Eu^{3+}(tta)_3Phen$ nanoparticles (3.7×10^{-6} M) were centrifuged to obtain the precipitate and then dissolved in 20% PBS solution in DMSO by ultrasonic vibration. Then 1 ml lysozyme solution (3.57×10^{-5} M) was added. The mixture was stirred at room temperature for 6 h and finally, the $Ag@SiO_2@Eu^{3+}(tta)_3Phen@lysozyme$ were obtained.

2.3. Characterisation: The fluorescent property was evaluated on a fluorescent spectrometer (Hitachi U-4100, Japan). The nanostructure of $Ag@SiO_2$, $Ag@SiO_2@Eu^{3+}(tta)_3Phen$ and $Ag@SiO_2@Eu^{3+}(tta)_3Phen@lysozyme$ was characterised by transmission electron microscopy (TEM, JEOL 2011, Japan) and high-resolution transmission electron microscopy (HRTEM, JEM-2100F, Japan). UV-visible spectrometer (Lambda 750, USA was used for UV–vis absorptions of samples. D8 (Bruker, Germany) X-ray diffractometer with graphite monochromator Cu Kα radiation ($\lambda = 1.54056$ nm) for the XRD test. Fourier Transform Infrared Spectrometer (NICOLET IS 50 FT-IR, U.S.A) was employed for the component measurement.

2.4. Blood compatibility test: Automatic hemagglutination analyser (ACLTOP 700, USA) was used for testing the blood compatibility of $Ag@SiO_2@Eu^{3+}(tta)_3Phen$ and $Ag@SiO_2@Eu^{3+}(tta)_3Phen@lysozyme$. First, 450 µl of fresh human blood plasma containing 50 µl 0.9%NaCl aqueous solution, sodium phosphate buffer, $Ag@SiO_2@Eu^{3+}(tta)_3Phen$ and $Ag@SiO_2@Eu^{3+}(tta)_3Phen@lysozyme$ compound was prepared. To avoid accidental errors, all test groups contain six test samples. After a two-hour reaction at 37°C, four full automatic clotting tests (prothrombin time, PT-S; partial thromboplastin time, APTT-S; thrombin time, TT-S; antithrombin-III time, AT-III) were performed. The blood plasma containing 0.9%NaCl aqueous solution is as a blank control group, the other three samples containing phosphate buffer, $Ag@SiO_2@Eu^{3+}(tta)_3Phen$ and $Ag@SiO_2@Eu^{3+}(tta)_3Phen@lysozyme$ were subjected to compared samples to be tested.

3. Results and discussion

3.1. Morphological structures of $Ag@SiO_2$, $Ag@SiO_2@Eu^{3+}(tta)_3Phen$ and $Ag@SiO_2@$ $Eu^{3+}(tta)_3Phen@lysozyme$: Fig. 2*a* shows

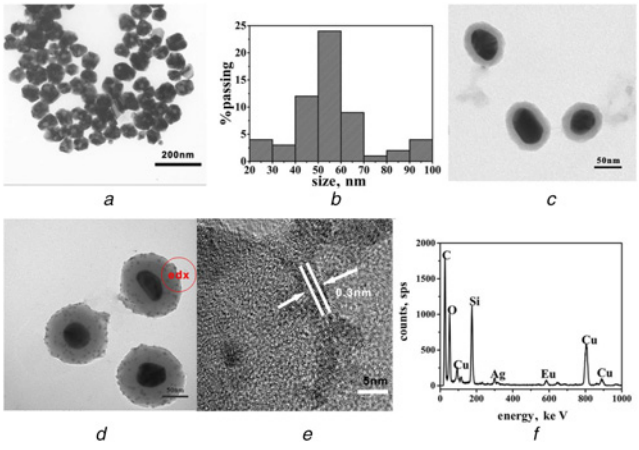

Fig. 2 *TEM images of*
a nanoAg
b Size distribution of Ag nanoparticles
c $Ag@SiO_2$nanospheres
d TEM image of $Ag@SiO_2@Eu(tta)_3Phen$
e HRTEM of $Ag@SiO_2@$ $Eu^{3+}(tta)_3Phen$ nanospheres
f EDS analysis the surface of $Ag@SiO_2@$ $Eu^{3+}(tta)_3Phen$

doi: 10.1049/mnl.2018.5130

the silver nanoparticles (nanoAg). The shapes are nearly spherical with the average diameter of 50–60 nm in Figs. 2*a*, *c* and *d*. Then, a layer of SiO_2 on the Ag cluster was achieved by in-situ hydrolysis and condensation of metal alkoxide precursors of tetraethoxysilane (TEOS). The TEOS molecules would interact rapidly with the water molecules inside the reverse micelles, forming partially hydrolysed species. Then these hydrolysed species would keep bound to the micelles due to their enhanced amphiphilic character brought about by the formation of silanol groups. The negative charge of the silica particles under alkaline conditions induces growth of the aggregate only around the edges of the Ag nanoparticles [35, 36]. Fig. 2*c* shows that the structure of SiO_2-covered nanoAg ($Ag@SiO_2$) has the coated-layer thickness of 25 nm. Therefore, the $Ag@SiO_2$ nanoparticles have the diameter of about 100 nm by using 50–60 nm nanoAg as cores.

Based on the indication of our publication [14], SiO_2 can hackle the electron transfer from the surface of nanoAg to its environment. Therefore, we can get the chance to make Eu^{3+} complex coverage at the surface of SiO_2 as a spacer. When the $Eu^{3+}(tta)_3Phen$ was added into the $Ag@SiO_2$ nanoparticles, the −OH groups of electron donors can have the interaction with the electron acceptor Eu^{3+} of complexes. Therefore, the Eu complex can be covalently linked to the silica shell [37]. Fig. 2*d* shows the TEM image of the triple nanostructure of $Ag@SiO_2@Eu^{3+}(tta)_3Phen$. The attachment of $Eu^{3+}(tta)_3Phen$ is stable at the surface of $Ag@SiO_2$. To prove this expectation, a high-resolution transmission electron microscope (HRTEM) test was carried out. As shown in Figs. 2*e* and *f*, the single $Eu^{3+}(tta)_3Phen$ behaves the crystal structure (Fig. 2*e*) and also EDS spectrum indicates the existence of C, O, Si, Ag and Eu^{3+}(Fig. 2*f*), which not only associates with the presence of nanoAg and SiO_2 spacer but also confirms the existence of Eu^{3+} in $Eu^{3+}(tta)_3Phen$. To impart the triple nanostructure biocompatible property, such as blood compatibility, this triple nanostructure was modified by a chosen protein, lysozyme. When we got the quadruple nanostructure of $Ag@SiO_2@Eu^{3+}(tta)_3Phen@lysozyme$,the amino acids of the lysozyme can incorporate with the Eu^{3+}. At the same time, the SiO_2 can also become the convenient carrier of proteins through the direct adsorption of lysozyme on silica surface [37]. Fig. 3*a* shows that there are obvious lysozyme floccules on the surface of the $Ag@SiO_2@$ $Eu^{3+}(tta)_3Phen$ nanoparticles, we think $Ag@SiO_2@$ $Eu^{3+}(tta)_3Phen@lysozyme$ was developed. Compared with Fig. 2*d*, it is believed that the lysozyme exists successfully on the surface of $Ag@SiO_2@Eu^{3+}(tta)_3Phen$. Fig. 3*b* presents an image of HRTEM for this quadruple nanostructure, in which the crystal lattice can be found. Thinking the possible reason, the lattice should from the crystalline of $Eu^{3+}(tta)_3Phen$ complex based on the observed interplanar space, i.e. 0.3 nm is the same as interplanar spacing data in Fig. 2*e*. Also, we infer this interplanar space is neither from protein, lysozyme nor from SiO_2. The former, lysozyme, shows the interplanar space, 1.8 nm [38, 39]. The later, SiO_2 is not crystalline as shown in Fig. 2*e*. The EDS data was shown in Fig. 3*c* and the existence of Eu^{3+} can be confirmed in this quadruple nanostructure, $Ag@SiO_2@Eu^{3+}(tta)_3Phen@lysozyme$. The peaks between 200 and 400 keV in Fig. 3*c* represent the Cl, K and S elements in lysozyme and buffer.

Fig. 3*d* shows the infrared spectra of $Ag@SiO_2@Eu^{3+}(tta)_3Phen$ (curve a), $Ag@SiO_2@$ $Eu^{3+}(tta)_3Phen@lysozyme$ (curve b) and the centrifugalised sample of $Ag@SiO_2@Eu^{3+}(tta)_3Phen@lysozyme$ (curve c). First, the curves a, b and c have a strong and sharp band at 1050 cm^{-1}, which indicates the asymmetrical vibration of Si–O–Si in SiO_2. The broad peak near 3375 cm^{-1} is assigned to the O–H characteristic peak of water. Then, the band near 1420 cm^{-1} is C–F telescopic vibration of TTA. The peak at 628 cm^{-1} is assigned to the telescopic vibration of Eu–O. Both of them are assigned to the $Eu^{3+}(tta)_3Phen$ complex. Correspondingly, compared with curve a, curve b has the typical absorption peak of the amide bond of lysozyme at 1660 cm^{-1}, which is assigned to the C=O telescopic vibration of the amide bond. The peak at 1309 cm^{-1} is the C–O telescopic vibration of the apical carboxyl group of lysozyme. At the same time, the peak at 709 cm^{-1} is the N–H external deformation vibration of lysozyme. All of them indicate the existence of the lysozyme. To dispel the influence of dissolved lysozyme in a solvent, $Ag@SiO_2@Eu^{3+}(tta)_3Phen@lysozyme$ was collected by centrifugation and was re-dissolved in a solvent (curve c in Fig. 3*d*). The typical characteristic peaks of lysozyme still exist at 1660 and 1309 cm^{-1}.

The XRD date was taken for the 2θ range of 10–80°. Fig. 4 shows the XRD patterns of the nanoAg, $Ag@SiO_2$ and $Ag@SiO_2@Eu^{3+}(tta)_3Phen$. The diffractogram has been compared with the standard powder diffraction card of JCPDS, silver Card No. 04-0783. Four peaks at 2θ values of 34.743°, 41.147°, 61.556°, and 74.945° in the experimental diffractogram have been identified to be due to silver metal and corresponding to (*hkl*) values (111), (200), (220) and (311) planes of silver [40]. In the $Ag@SiO_2@Eu^{3+}(tta)_3Phen$, the new peaks at 17.559,

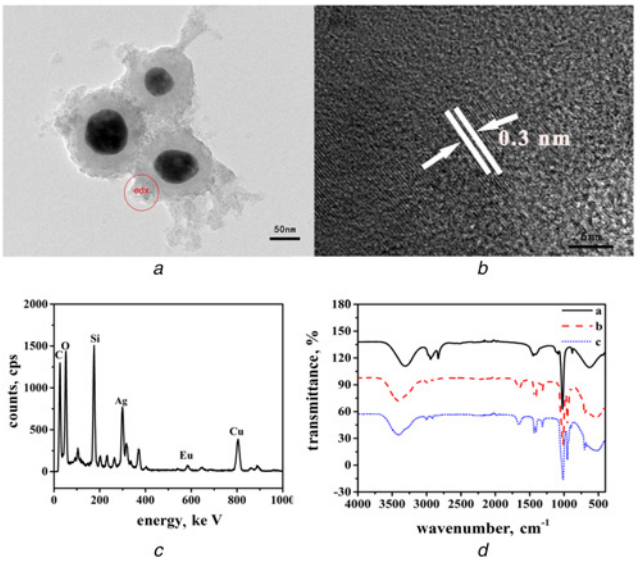

Fig. 3 *Nanostructural and compositional analyses of quadruple $Ag@SiO_2@Eu^{3+}(tta)_3Phen@lysozyme$*
a TEM image of $Ag@SiO_2@Eu^{3+}(tta)_3Phen@lysozyme$
b HRTEM of $Ag@SiO_2@Eu^{3+}(tta)_3Phen@lysozyme$ nanoparticles
c EDS analysis the surface of $Ag@SiO_2@Eu^{3+}(tta)_3Phen@lysozyme$ nanoparticles
d Infrared spectroscopies: (curve a)$Ag@SiO_2@Eu^{3+}(tta)_3Phen$, (curve b) $Ag@SiO_2@$ $Eu^{3+}(tta)_3Phen@lysozyme$ and (curve c) $Ag@SiO_2@Eu^{3+}(tta)_3Phen@lysozyme$ after centrifugation

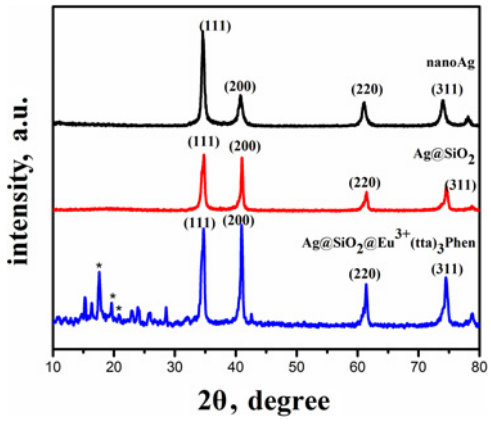

Fig. 4 *XRD test of nanoAg, $Ag@SiO_2$ and $Ag@SiO_2@Eu^{3+}(tta)_3Phen$*

19.449 and 20.999 were the typical peaks of the Eu complex, which are consistent with the previous report [41].

3.2. UV–vis absorption of $Ag@SiO_2@Eu^{3+}(tta)_3Phen$: Fig. 5 presents the UV–vis characteristic absorptions of nanoAg (spectrum a), $Ag@SiO_2$ (spectrum b), $Ag@SiO_2@Eu^{3+}(tta)_3Phen$ (spectrum c). We can find that nanoAg has a maximum absorption at 456 nm (spectrum a), whereas $Ag@SiO_2$ has the maximum adsorption at 480 nm (spectrum b), that red-shifts 24 nm comparing the adsorption with naked nanoAg because SiO_2 covering makes the stabilisation effect. The large difference is in spectrum c, which is the characteristic adsorption of $Ag@SiO_2@Eu^{3+}(tta)_3Phen$. When $Eu^{3+}(tta)_3Phen$ shells the $Ag@SiO_2$ nanoparticles, the absorption peaks at 260 and 342 nm occur, which is attributed to the adsorption of organic light antenna TTA and Phen. Correspondingly, the adsorption of $Ag@SiO_2$ at 480 nm shows a much broadened peak.

3.3. Investigation of fluorescent property of $Ag@SiO_2@Eu^{3+}(tta)_3$-Phen and $Ag@SiO_2@$ $Eu^{3+}(tta)_3Phen@lysozyme$: As expected, due to the very weak emission of $Eu^{3+}Cl_3{\cdot}6H_2O$, the antenna effect of TTA and Phen is needed to enhance both excitation and emission, which means the co-antenna effect of TTA and Phen.

As shown in Fig. 6, TTA and Phen as incident light harvesting compounds accept light energy and were excited into their singlet states, S_{1TTA} and S_{1Phen} levels. After they experienced the transform from singlet states to triplet states T_{1TTA} and T_{1Phen}, the energy harvested by TTA and Phen was transferred to the excited state of Eu^{3+}, $^5D_0$. Through these energy transfer processes, the emission of Eu^{3+} was enhanced largely. TTA and Phen molecules significantly reduce the non-radiative channels by replacing water molecules [42]. When the $Ag@SiO_2@Eu^{3+}(tta)_3Phen$ nanoparticle was obtained, the SiO_2 shell can prevent nanoAg from interfering with the environment and hinder the oxidation of the Ag surface and nanoparticle aggregation. It significantly improves the fluorescence intensity by MEF effect (embedded figure of Fig. 6).

Based on the excitation and emission characteristics of $Eu^{3+}(tta)_3Phen$ complex, SPR-effect from nanoAg was further introduced into this complex system. Because the naked nanoAg is harmful to the fluorescent property of $Eu^{3+}(tta)_3Phen$ complex [15], the SiO_2-covered nanoAg, was introduced. Figs. 7*a* and *b* present the excitation and emission spectra of (a) $Eu^{3+}(tta)_3Phen$, (b) $Ag@SiO_2@Eu^{3+}(tta)_3Phen$ and (c) $Ag@SiO_2@Eu^{3+}(tta)_3$-Phen@lysozyme. We can find that $Ag@SiO_2$ core/shell nanostructure can largely enhance both of excitation and emission spectra of $Eu^{3+}(tta)_3Phen$ complex in triple nanostructure of

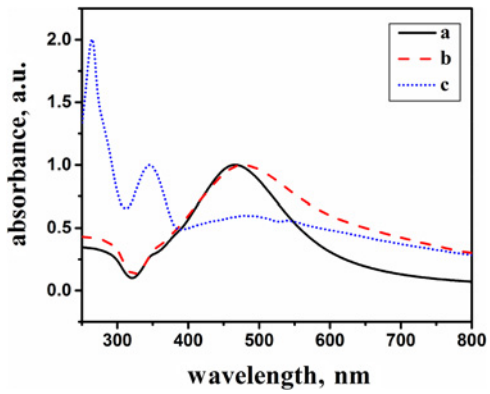

Fig. 5 *UV–vis spectra*
a Ag nanoparticles
b $Ag@SiO_2$ particles
c $Ag@SiO_2@$ $Eu^{3+}(tta)_3Phen$

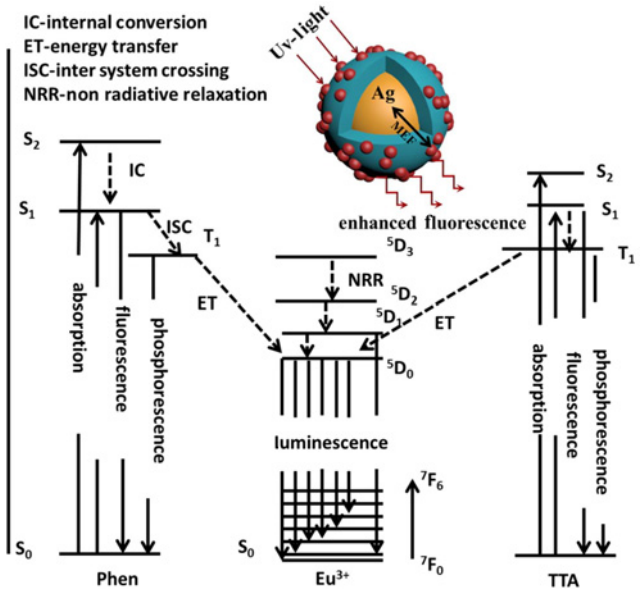

Fig. 6 *Schematic energy level diagram showing energy transfer process and different transitions in the. $Eu^{3+}(tta)_3Phen$; the enhanced fluorescence schematic graph of the core–shell nanoparticle (embedded)*

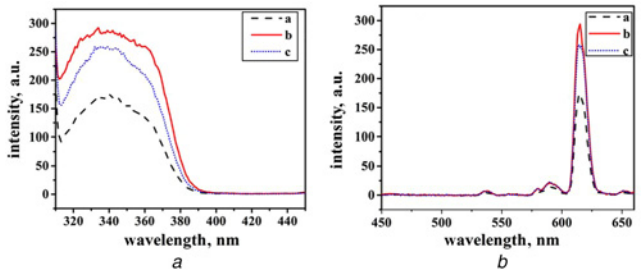

Fig. 7 *Excitation and emission fluorescent spectra*
a Excitation spectra
b Emission spectra.
In both (a) and (b), curve a, curve b and curve c spectra correspond the samples of $Eu^{3+}(tta)_3Phen$, $Ag@SiO_2@Eu^{3+}(tta)_3Phen$ and $Ag@SiO_2@Eu^{3+}(tta)_3Phen@lysozyme$, respectively

$Ag@SiO_2@Eu^{3+}(tta)_3Phen$ in spectrum b in Figs. 7*a* and *b* correspondingly.

Furthermore, in spectrum c of Figs. 7*a* and *b*, when lysozyme was attached at the surface of $Eu^{3+}(tta)_3Phen$ to develop into the quadruple nanostructure of $Ag@SiO_2@Eu^{3+}(tta)_3Phen@lysozyme$, both the excitation and emission intensities slightly decreased by about 10%. This can be attributed to the multi-washing and centrifugation for solvent change in the preparation process of the quadruple nanostructure. In the measurement of excitation and emission Figs. 7*a* and *b*, the optimal excitation wavelengths were obtained by scanning with a maximum emission wavelength of Eu^{3+} emission at 615 nm, correspondingly, the optimal emission spectra were obtained by the optimal excitation wavelength at 342 nm. Both the emission and excitation slits are 5 nm. Because the extremely low concentration of the complexes, the enhancement effect of the $Ag@SiO_2@Eu^{3+}(tta)_3Phen$ is not satisfactory. We hope to solve this defect in the subsequent study.

3.4. Evaluations of anti-coagulation of human blood plasma: Prothrombin time (PT) referring to the time needed for the plasma coagulation after prothrombin is converted into thrombin in the plasma without blood platelet. Its clinical reference value is 8–14 s. We used the human blood plasma as a test system

doi: 10.1049/mnl.2018.5130

and the PT-S values of 0.9%NaCl aqueous solution and phosphate buffer as reference additives, in which the former is the clinical anti-coagulation agent and the latter is our solvent system of the quadruple nanostructure of $Ag@SiO_2@Eu^{3+}(tta)_3Phen@lysosyme$. As we can see from Fig. 8*a*, the PT-S values of blood plasmas with the additions of 0.9%NaCl aqueous solution and phosphate buffer are close, but the value of blood plasma with the addition of $Ag@SiO_2@Eu^{3+}(tta)_3Phen$ has longer time that indicated its negative effect, which should be caused by the $Eu^{3+}(tta)_3Phen$ surface nature. However, in Fig. 8*e*, when $Ag@SiO_2@Eu^{3+}(tta)_3Phen$ was modified by lysozyme (a popular protein) to form the quadruple nanostructure of $Ag@SiO_2@Eu^{3+}(tta)_3Phen$ @lysozyme, the PT-S value is fairly close to the values of 0.9%NaCl aqueous solution and phosphate buffer as reference additives. The correlation coefficient is 0.994 referring to sample II in Table 1. This result confirms that protein (lysozyme) makes the surface of the quadruple nanostructure of $Ag@SiO_2@Eu^{3+}(tta)_3Phen@lysosyme$ has good blood compatibility. The second parameter that is normally evaluated is APTT-S, which is the standard activated partial thromboplastin time, whose clinical reference value is 24–42%.

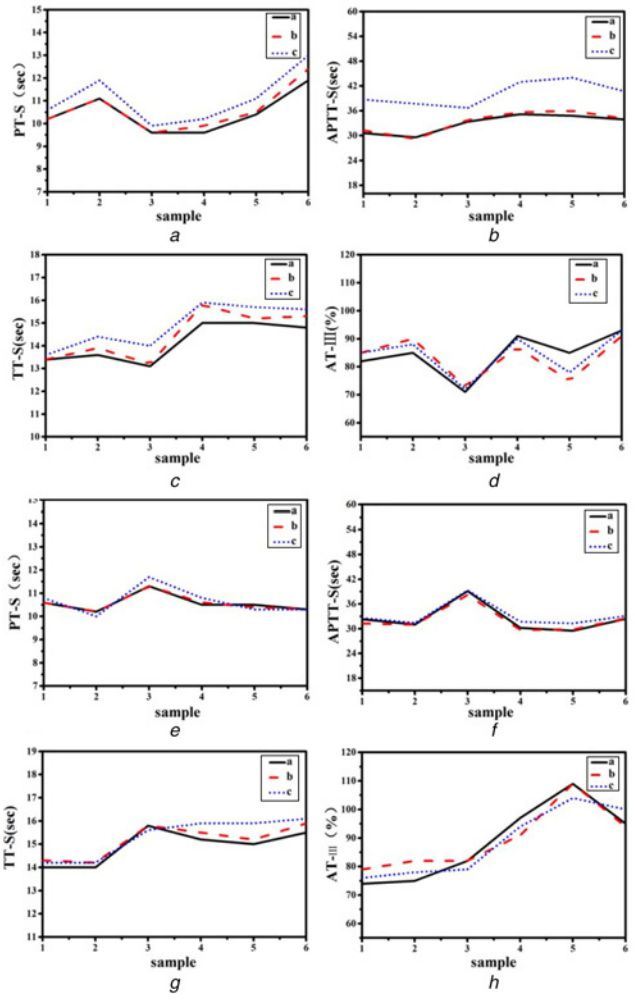

Fig. 8 *Evaluations of anti-coagulation of human blood plasma with PT-S, APTT-S, TT-S and AT-III*
a–d Results of $Ag@SiO_2@Eu^{3+}(tta)_3Phen$ sample, in which curve a is the reference physiological saline state (0.9%NaCl aqueous solution, curve b is the solvent of lysozyme: phosphate buffer and curve c is the $Ag@SiO_2@Eu^{3+}(tta)_3Phen$ sample
e–h Results of $Ag@SiO_2@$ $Eu^{3+}(tta)_3Phen@lysozyme$ sample, in which curve a is the reference physiological saline state (0.9%NaCl aqueous solution, curve b is the solvent of lysozyme: phosphate buffer and curve c is the $Ag@SiO_2@$ $Eu^{3+}(tta)_3Phen@lysozyme$ sample

Table 1 Correlation coefficients[a] of blood plasmas containing phosphate buffer (solvent), $Ag@SiO_2@Eu^{3+}(tta)_3Phen$ (sample I), $Ag@SiO_2@$ $Eu^{3+}(tta)_3Phen@lysozyme$ (sample II)

Project	Solvent	Sample I	Sample II
PT-S	0.984	0.796	0.994
APTT-S	0.986	0.715	0.987
TT-S	0.982	0.674	0.967
AT-III	0.946	0.975	0.963

[a]Note: The values are to correlate to the physiological saline state (0.9% NaCl aqueous solution).

We can see from Fig. 8*b* that the value of blood plasma with the addition of $Ag@SiO_2@Eu^{3+}(tta)_3Phen$ (sample I in Table 1) diverges from the values of blood plasma including 0.9%NaCl aqueous solution and phosphate buffer. Whereas, in Fig. 8*f*, the value of APTT-S regarding the blood plasma including quadruple nanostructure of $Ag@SiO_2@Eu^{3+}(tta)_3Phen@lysosyme$ has a high consistency with the values in the physiological saline state(0.9%NaCl aqueous solution), which shows the high antithrombinability. The third parameter to be observed is TT-S (thrombin time) refers to the time that fibrinogen turns into fibrin. In Figs. 8*c* and *g*, the TT-S value of $Ag@SiO_2@Eu^{3+}(tta)_3Phen@lysozyme$ sample shows a better anastomotic behaviour than the value of $Ag@SiO_2@Eu^{3+}(tta)_3Phen$ sample. The fourth parameter is AT-III that is mainly secreted by hepatocytes and vascular endothelial cells. It is the main physiological anticoagulant in human plasma, which accounts for 50–70% of the total plasma antithrombin activity. Figs. 8*d* and *g* indicate the distributions of $Ag@SiO_2@Eu^{3+}(tta)_3Phen$ and $Ag@SiO_2@Eu^{3+}(tta)_3Phen@$-lysozyme samples referring to the 0.9% NaCl aqueous solution and phosphate buffer, obviously, the sample of $Ag@SiO_2@Eu^{3+}(tta)_3Phen@lysozyme$ has better anastomose in total six measurements, although the correlation coefficient is a little bit lower (in Table 1). All the correlation coefficients were listed in Table 1, and we can find that the blood plasma containing $Ag@SiO_2@Eu^{3+}(tta)_3Phen@lysozyme$ has better correlation parameters and the values are much closer to the values of the physiological saline state (0.9% NaCl aqueous solution). As the comment, protein modified quadruple nanostructure has good blood compatibility and it can be applied in human blood system to work for bio-imaging or to develop new generation sensors such as metal ion detection and temperature induction sensors [41, 42]. At the same time, a series of excellent properties of rare earth ions such as Tm, Tb, Er, Dy have the property of different emission spectra and sharp peak, which is hopeful to be used in the field of biosensor applications [43].

4. Conclusion: To increase the luminescent property of $Eu^{3+}(tta)_3$-Phen, triple nanostructure, $Ag@SiO_2@Eu^{3+}(tta)_3Phen$, was designed to utilise the SPR effect. As results, the fluorescence intensities of the triple nanostructure of $Ag@SiO_2@Eu^{3+}(tta)_3Phen$ and quadruple nanostructure of $Ag@SiO_2@Eu^{3+}(tta)_3Phen@$-lysozyme were significantly enhanced. Especially, the modification of lysozyme at the surface of the triple nanostructure, $Ag@SiO_2@$-$Eu^{3+}(tta)_3Phen$ can implement to enhance the biocompatibility of final quadruple nanostructure. Very importantly, the anticoagulant tests with the parameters of PT-S, APTT-S, TT-S and AT-III indicated the excellent anticoagulant effect of the quadruple nanostructure of $Ag@SiO_2@Eu^{3+}(tta)_3Phen@lysozyme$. Therefore, we can expect the great potential applications in the field of biological protein detection technology, such as bio-imaging and bio-sensing in in vivo body.

5. Acknowledgments: This work was supported by (1) the Natural Scientific Foundation of China (grant no. 51473082), (2) State Key Project of International Cooperation Research (grant nos. 2017YFE0108300, 2016YFE0110800); (3) the Program for Introducing Talents of Discipline to Universities ('111' plan); (4) the first class disciplines of Shandong Province; (5) the National One-Thousand Foreign Expert Program (grant no. WQ20123700111).

6 References

[1] Wang X., Tang J., Xu Q., *ET AL.*: 'Fluorescent polymeric aggregates induced by Eu^{3+} ions and their surface morphologies', *Opt. Mater.*, 2015, **46**, pp. 28–33

[2] Binnemans K.: 'Lanthanide-based luminescent hybrid materials', *Chem. Rev.*, 2009, **109**, (9), pp. 4283–4374

[3] Eliseeva S.V., Buenzli J.C.G.: 'Cheminform abstract: rare earths: jewels for functional materials of the future', *Cheminform*, 2011, **42**, (37), pp. 1165–1176

[4] Binnemans K.: 'Interpretation of Europium(III) spectra', *Coord. Chem. Rev.*, 2015, **295**, pp. 1–45

[5] Liang F., Zhou Q., Cheng Y., *ET AL.*: 'Oxadiazole-functionalized Europium(III) β-diketonate complex for efficient red electroluminescence', *Chem. Mater.*, 2003, **15**, (2003), pp. 1935–1937

[6] Tsuda N., Okada M., Murakami T.: 'Potential of gadolinium-ethoxybenzyl-diethylenetriamine pentaacetic acid (Gd-EOB-DTPA) for differential diagnosis of nonalcoholic steatohepatitis and fatty liver in rats using magnetic resonance imaging', *Invest. Radiol.*, 2007, **42**, (4), p. 242

[7] Wang L., Song Y.: 'Anti-tumor activity of rare earth-curcumin-pyridine/2,2-bipyridine/1, 10-phenanthroline complexes', *J. Chin. Soc. Rare Earths*, 2014, **32**, (1), pp. 50–60

[8] Liu S., Yan L., Yang R.: 'Preparation and properties of rare earths with 6-methyl-2-picolinic acid N oxide and 2,2′-bipyridine N,N′-dioxide', *J. Rare Earth*, 2000, **18**, (2), pp. 81–85

[9] Sager W.F., Filipescu N., Serafin F.A.: 'Substituent effects on intramolecular energy transfer. I. Absorption and phosphorescence spectra of rare earth β-diketone chelates', *J. Phys. Chem.*, 1965, **69**, (4), pp. 1092–1100

[10] Bünzli J.C., Piguet C.: 'Taking advantage of luminescent lanthanide ions', *Chem. Soc. Rev.*, 2005, **34**, (12), p. 1048

[11] Zhao S., Zhang L., Li W., *ET AL.*: 'Preparation and fluorescent property of Eu(TTA)3Phen incorporated in polycarbonate resin', *Polym. J.*, 2006, **38**, (6), pp. 523–526

[12] Pei J., Liu X., Yu W., *ET AL.*: 'Efficient energy transfer to achieve narrow bandwidth red emission from Eu^{3+}-grafting conjugated polymers', *Macromolecules*, 2002, **35**, (19), pp. 7274–7280

[13] Di Lorenzo M.L., Cocca M., Gentile G., *ET AL.*: 'Thermoreversible luminescent organogels doped with Eu(TTA)3phen complex', *J. Colloid Interface Sci.*, 2013, **398**, (19), pp. 95–102

[14] Wang A.L., Zhou D., Wei X.Y., *ET AL.*: 'Luminescence properties and crystal structure of europium complexes with phenoxyacetic acid and 2,4,6-tri(2-pyridyl)-s-triazine', *J. Lumin.*, 2015, **160**, pp. 238–244

[15] Ray K., Badugu R., Lakowicz J.R.: 'Distance-dependent metal-enhanced fluorescence from Langmuir–Blodgett monolayers of alkyl-NBD derivatives on silver island films', *Langmuir ACS J. Surf. Colloids*, 2006, **22**, (20), pp. 8374–8378

[16] Zhou J., Li B., Lu S., *ET AL.*: 'Regulation of osteoblast proliferation and differentiation by interrod spacing of Sr-HA nanorods on microporous titania coatings', *ACS Appl. Mater. Interfaces*, 2013, **5**, (11), pp. 5358–5365

[17] Shen W., Tang J., Wang D., *ET AL.*: 'Enhanced efficiency of polymer solar cells by structure-differentiated silver nano-dopants in solution-processed tungsten oxide layer', *Mater. Sci. Eng. B*, 2016, **206**, pp. 61–68

[18] Zhang H.X., Lin X.M., Wang A.L., *ET AL.*: 'Fluorescence enhancement of europium complexes by core-shell $Ag@SiO_2$ nanoparticles', *Spectrochim. Acta A, Mol. Biomol. Spectrosc.*, 2015, **151**, pp. 716–722

[19] Kang J., Li Y., Chen Y., *ET AL.*: 'Core–shell $Ag@SiO_2$ nanoparticles of different silica shell thicknesses: preparation and their effects on photoluminescence of lanthanide complexes', *Mater. Res. Bull.*, 2015, **71**, (9), pp. 116–121

[20] Zhuo S., Shao M., Cheng L., *ET AL.*: 'Surface-enhanced fluorescence from copper nanoparticles on silicon nanowires', *Front. Optoelectron. Chin.*, 2011, **4**, (1), p. 114

[21] Zhang Y., Wang X., Tang J., *ET AL.*: 'Strong enhancement effect of silver nanowires on fluorescent property of Eu3+-ligand complexes and desired fluorescent iPP composite materials', *Opt. Mater.*, 2017, **66**, pp. 17–22

[22] St John K.R.: 'Biocompatibility of dental materials', *Alpha Omegan*, 1988, **81**, (4), pp. 20–24

[23] Chung J.W., Gerelkhuu Z., Ju H.O., *ET AL.*: 'Recent advances in luminescence properties of lanthanide-doped up-conversion nanocrystals and applications for bio-imaging, drug delivery, and optosensing', *Appl. Spectrosc. Rev.*, 2016, **51**, (7–9), pp. 00–00

[24] Zhao H., Cheng Z., Hu R., *ET AL.*: 'Oxidative injury in the brain of mice caused by Lanthanide', *Biolog. Trace Element Res.*, 2011, **142**, (2), pp. 174–189

[25] Chung C., Deák F., Kavalali E.T.: 'Molecular substrates mediating lanthanide-evoked neurotransmitter release in central synapses', *J. Neurophysiol.*, 2008, **100**, (4), pp. 2089–2100

[26] Deng W., Jin D., Drozdowicz-Tomsia K., *ET AL.*: 'Ultrabright Eu–doped plasmonic $Ag@SiO_2$ nanostructures: time-gated bioprobes with single particle sensitivity and negligible background', *Adv. Mater.*, 2011, **23**, (40), pp. 4649–4654

[27] Wang Z.Z., Zhan L.Q., Chen X.X.: 'Two types of lysozymes from the whitefly *Bemisia tabaci*: molecular characterization and functional diversification', *Dev. Comparative Immunol.*, 2018, **81**, pp. 252–261

[28] Lysozyme F.O.: 'Folding of lysozyme', 1996

[29] Ogasahara K., Hamaguchi K.: 'Structure of lysozyme: XII. Effect of pH on the stability of lysozyme', *J. Biochem.*, 1967, **61**, (2), p. 199

[30] Varma D.R.: 'Influence of dietary protein on the disposition and metabolism of phen', *Can. J. Physiol. Pharmacol.*, 1980, **58**, (3), pp. 231–236

[31] Song Y.Y., Xu Y.Z., Weng S.F., *ET AL.*: 'Biological effects of rare earth protein complexes: influence of lanthanide ions Eu3+, Tb3+ on secondary structure of calmodulins', *Biospectroscopy*, 1999, **5**, (6), pp. 371–377

[32] Guo C., Wu X., Xu W., *ET AL.*: 'Resonance light-scattering enhancement effect of the protein-Y3+-TTA-SLS system and its analytical application', *Luminescence*, 2008, **23**, (6), p. 404

[33] Barrera E.G., Livotto P.R., Santos J.H.Z.D.: 'Hybrid silica bearing different organosilanes produced by the modified Stöber method', *Powder Technol.*, 2016, **301**, pp. 486–492

[34] Xu Q., Tang J., Wang Y., *ET AL.*: 'Eu(3 +)-induced aggregates of diblock copolymers and their photoluminescent property', *J. Colloid Interface Sci.*, 2013, **394**, p. 630

[35] Aslan K., Wu M., Lakowicz J.R., *ET AL.*: 'Fluorescent core-shell $Ag@SiO_2$ nanocomposites for metal-enhanced fluorescence and single nanoparticle sensing platforms', *J. Am. Chem. Soc.*, 2007, **129**, (6), pp. 1524–1525

[36] Bae D.S., Park S.W., Han K.S., *ET AL.*: 'Synthesis of Ag/SiO_2 nanosize particles by reverse micelle and sol-gel processing', *Metals Mater. Interfaces*, 2001, **7**, (4), pp. 399–402

[37] Lechner C.C., Becker C.F.: 'Immobilising proteins on silica with site-specifically attached modified silaffin peptides', *Biomater. Sci.*, 2015, **3**, (2), pp. 288–297

[38] England M.W., Lambert E.M., Li M., *ET AL.*: 'Fabrication of polypyrrole nano-arrays in lysozyme single crystals', *Nanoscale*, 2012, **4**, (21), pp. 6710–6713

[39] Guli M., Lambert E.M., Li M., *ET AL.*: 'Template-directed synthesis of nanoplasmonic arrays by intracrystalline metalization of cross-linked lysozyme crystals', *Angew Chem. Int. Ed. Engl.*, 2010, **49**, (3), pp. 520–523

[40] Purushotham E., Krishna N.G.: 'Preparation and characterization of silver nano particles', *Indian J. Phys.*, 2014, **88**, (2), pp. 157–163

[41] Wang Y., Huang L., Tang J., *ET AL.*: 'Luminescent polyacrylonitrile (PAN) electrospinning nanofibers encapsulating silica nanoparticles carried ternary Europium complex', *Int. J. Electrochem. Sci.*, 2016, **11**, pp. 2058–2065

[42] Shahi P.K., Singh A.K., Singh S.K., *ET AL.*: 'Revelation of the technological versatility of the Eu(TTA)3Phen complex by demonstrating energy harvesting, ultraviolet light detection, temperature sensing, and laser applications', *ACS Appl. Mater. Interfaces*, 2015, **7**, (33), pp. 18231–18239

[43] Wang J., Lv M., Wang Z., *ET AL.*: 'Highly sensitive and selective fluorescent detection of rare earth metal Sn(II) ion by organic fluorine Schiff base functionalized periodic mesoporous material in aqueous solution', *J. Photochem. Photobiol. A Chem.*, 2015, **309**, pp. 37–46

doi: 10.1049/mnl.2018.5130